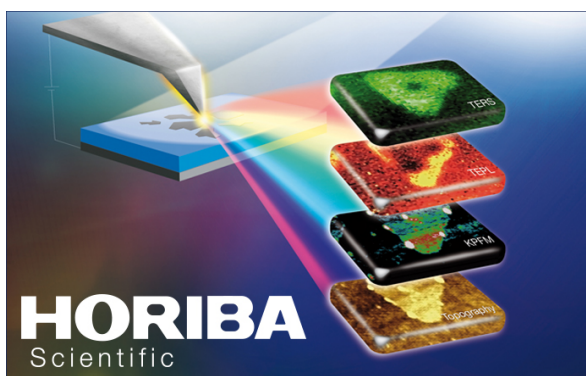


PAPER

Conductive connection induced speed-up of localized-surface-plasmon dynamics

To cite this article: Peng Cun *et al* 2018 *J. Opt.* **20** 014011

View the [article online](#) for updates and enhancements.



LIVE WEBINAR

NanoRaman: Correlated Tip-Enhanced Optical Spectroscopy and Scanning Probe Microscopy

Thursday 8 March 15.00 GMT

REGISTER NOW!

physicsworld.com

Conductive connection induced speed-up of localized-surface-plasmon dynamics

Peng Cun¹, Meng Wang¹, Cuiying Huang¹, Pei Huang^{2,3}, Xinkui He², Zhiyi Wei² and Xinp ing Zhang¹ 

¹Institute of Information Photonics Technology and College of Applied Sciences, Beijing University of Technology, Beijing, 100124, People's Republic of China

²Institute of Physics, Chinese Academy of Sciences, Beijing National Lab of Condensed Matter Physics, Beijing, 100190, People's Republic of China

³Xi'an Institute of Optics and Fine Mechanics, Chinese Academy of Sciences, Xi'an, 710119, People's Republic of China

E-mail: zhangxinping@bjut.edu.cn

Received 11 August 2017, revised 1 December 2017

Accepted for publication 5 December 2017

Published 27 December 2017



CrossMark

Abstract

Conductive connection of localized surface plasmons (LSPs) was achieved by depositing a layer of continuous gold film onto the top surface of a matrix of randomly distributed gold nanoparticles (AuNPs) that were originally isolated on a glass substrate. Ultrafast spectroscopic response of such plasmonic nanostructures was investigated by femtosecond pump-probe detection technique. The transient-absorption data showed large redshift and broadening of the resonance spectrum of the conductively connected AuNPs with respect to the isolated ones. Such effects led to modulation on the evolution dynamics of LSPs in a transient transition spectral band. Making use of the temporal and spectral dislocation between the edges of transition band, we achieved much increased speed of the plasmonic optical switching effect.

Keywords: transient absorption spectroscopy, localized surface plasmon resonance, continuous gold film, gold nanoparticles, plasmonic optical switch

(Some figures may appear in colour only in the online journal)

1. Introduction

Localized surface plasmon resonance (LSPR) is dependent on the shape, size, and composition of the metallic nanostructures [1–5]. The dielectric constant of the environmental medium is another essential factor that influences the spectroscopic response of the plasmonic nanostructures [6–8], which is the basis for the plasmonic sensors and ultrafast optical switching devices. Hybridization between LSPR and surface plasmon polaritons (SPP) is an effective approach to enhance the functions or extend the potential applications of the devices [9–11]. Such hybrid plasmons can be achieved by combining continuous metallic films with isolated nanostructures. Special photophysical effects or functions may be achieved through coupling between LSPR and SPP. Physics involved in the interaction between the metallic nanoparticles and thin films have been studied experimentally in a progressively elongated silver nanoparticle and a silver film [12]

and theoretically in the system consisting of a gold nanoparticle (AuNP) and a gold film with adjustable separation distance [13]. In particular, the electron–electron and electron–phonon interactions in LSPR [14, 15] and in the hybrid systems [10, 11] can be utilized to achieve ultrafast optical switching devices. In this work, we investigate how a continuous gold film (AuFilm) deposited on the top surface of the isolated AuNPs influences the steady-state and ultrafast-spectroscopic response of LSPR of such conductively connected AuNPs (CCAuNPs) sitting on a glass substrate.

2. AuNPs connected by a continuous gold film

AuNPs in the size ranging from 5 to 10 nm were first synthesized chemically and the colloidal solution was prepared by suspending them in xylene with a concentration of 100 mg ml⁻¹. Then, the colloidal solution was spin-coated at

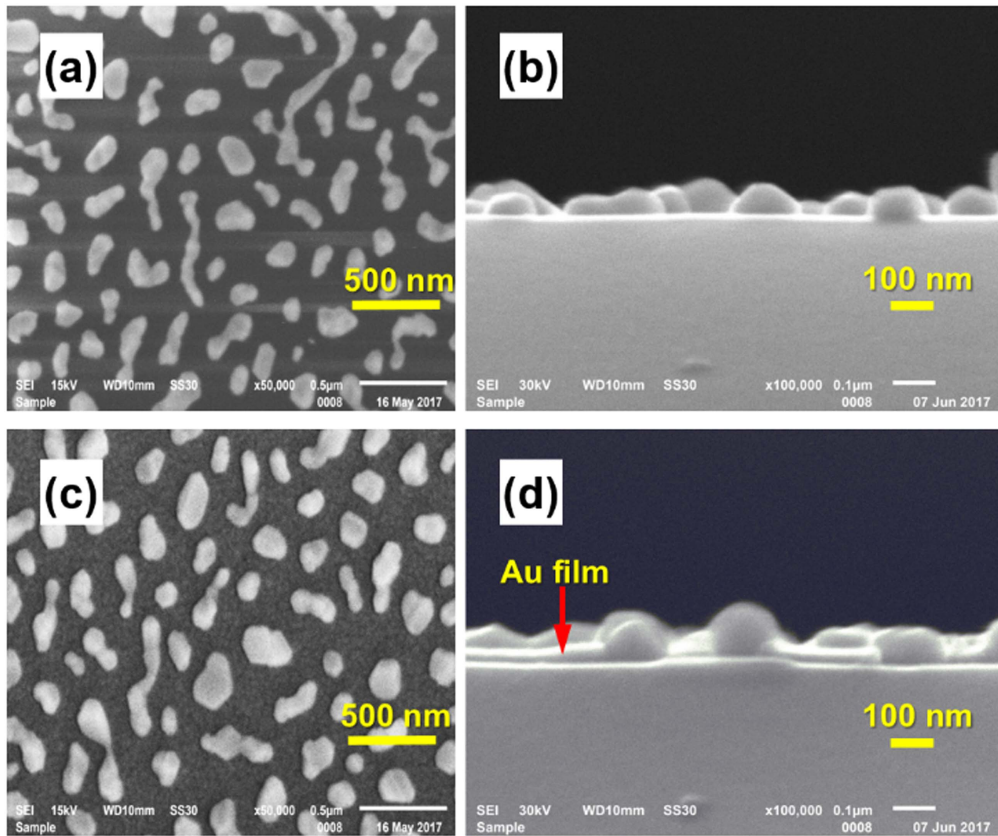


Figure 1. (a), (b) Top view and cross-sectional SEM images of the gold nanoparticles, respectively. (c), (d) Top view and cross-sectional SEM images, respectively, after the gold nanoparticles are coated with a layer of 40 nm-thick gold film.

a speed of 2000 rpm for 30 s onto a silica substrate with an area of $20 \times 20 \text{ mm}^2$. The sample was then annealed in vacuum in a muffle furnace at a temperature about $500 \text{ }^\circ\text{C}$ for 10 min, as has been described in our previous work [16, 17], to produce isolated and randomly distributed AuNPs on the substrate of fused silica. Figures 1(a) and (b) show the top and cross-sectional views of the scanning electron microscopic (SEM) images of the produced AuNPs, respectively, showing irregularity in their shapes and large-range distribution in their sizes.

A layer of continuous gold film was then deposited onto the random matrix of AuNPs by thermal evaporation. We have tried different thicknesses of the gold film, ranging from 20 to 60 nm. However, a thickness of 40 nm not only supplied an excellent continuity, but also enabled reliable measurements on the transmissive optical extinction spectra. Therefore, we employed a thickness of 40 nm for the continuous gold film for all of the experimental work demonstrated in this manuscript. Figures 1(c) and (d) show the top and cross-sectional views of the SEM images of the AuNPs after they were coated with a 40 nm-thick gold film, respectively, which are termed as CCAuNPs. The gold film is indicated in figure 1(d) by a downward red arrow.

3. Steady-state spectroscopic characterization on the modification by the conductive connection

Figure 2 shows the optical extinction spectra measured on the isolated AuNPs (solid blue) and the CCAuNPs (solid black). For

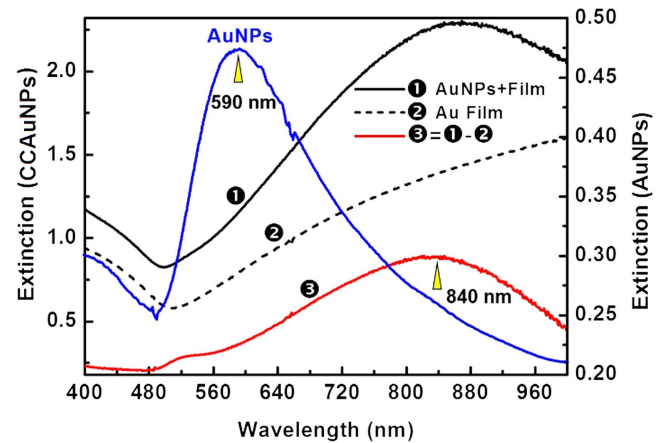


Figure 2. Optical extinction spectra measured on the gold nanoparticles before (blue) and after (black, ①) they are coated with a 40 nm gold film. The dashed black curve (②) shows the measurement on a 40 nm gold film deposited on a glass substrate. The red curve (③) shows the difference between ① and ②.

comparison, measurements have also been performed on the AuFilm with the same thickness as that deposited on the AuNPs, as shown by the dashed black curve in figure 2. The red spectrum (③) in figure 2 shows the difference between the extinction spectra of the CCAuNPs (①) and the AuFilm (②) with $\text{③} = \text{①} - \text{②}$. This can be understood by considering the definition of optical extinction spectrum, which was calculated by

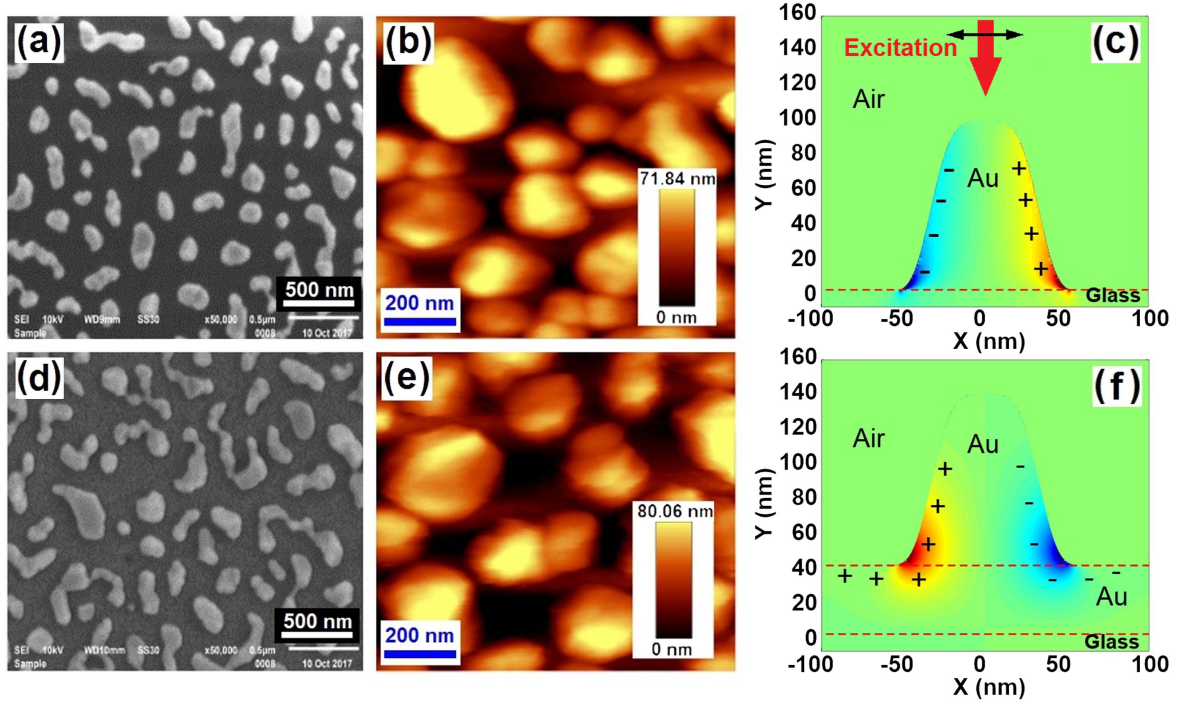


Figure 3. (a), (b) SEM and AFM images of the AuNPs. (c) Calculated plasmonic charge distribution in the AuNPs under optical excitation along the normal of the glass substrate. (d), (e) SEM and AFM images of the CCAuNPs. (f) Calculated plasmonic charge distribution in the CCAuNPs under optical excitation along the normal of the glass substrate.

$-\log_{10} \frac{I_{\text{CCAuNPs}}(\lambda)}{I_0(\lambda)}$ (1) and $-\log_{10} \frac{I_{\text{AuFilm}}(\lambda)}{I_0(\lambda)}$ (2) for the CCAuNPs and the AuFilm, respectively, with $I_{\text{CCAuNPs}}(\lambda)$, $I_{\text{AuFilm}}(\lambda)$, and $I_0(\lambda)$ defined as the reflection spectrum by the CCAuNPs, the reflection spectrum by the AuFilm, and the blank spectrum, respectively. Thus, the difference spectrum calculated by $\left[-\log_{10} \frac{I_{\text{CCAuNPs}}(\lambda)}{I_0(\lambda)}\right] - \left[-\log_{10} \frac{I_{\text{AuFilm}}(\lambda)}{I_0(\lambda)}\right] = -\log_{10} \frac{I_{\text{CCAuNPs}}(\lambda)}{I_{\text{AuFilm}}(\lambda)}$ (3) is approximately the optical extinction spectrum of the CCAuNPs with the reflection spectrum by the AuFilm used as the blank. The above discussions also explain the relationship between the spectra in figure 2.

According to figure 2, the conductive connection has led to a red-shift of the peak wavelength of the LSPR spectrum from 590 to 840 nm and a broadening of the bandwidth of the resonance spectrum at FWHM from about 190 to 310 nm. Meanwhile, the spectral amplitude at the peak wavelength was increased from about 0.47 to 0.89 OD (optical density), implying much enhancement of optical extinction by the LSP through conductive connection.

Looking back at figures 1(b) and (d), we can observe that the coating of 40 nm gold film has resulted in the enlargement of the AuNPs without increasing largely their relative heights. The relative heights can be obtained by subtracting the thickness of the gold film from the absolute heights of the CCAuNPs. Figures 3(a) and (b) show the SEM and AFM images of the AuNPs, respectively, which were measured on a different site from that of figure 1. Figures 3(d) and (e) show those of the CCAuNPs. Further comparison in figure 3 enable us to verify small change (<10 nm) in the relative height of the AuNPs after they were coated with a continuous gold film, while the diameters of the AuNPs were increased. This

implies reduced height/diameter ratios and explains partly the red-shifted LSPR spectrum. Furthermore, LSPR in the CCAuNPs also induced redistribution of the free charge carriers in the surrounding planar gold film. Such a mechanism can be verified by the theoretical simulation of the charge distributions in the isolated AuNPs and the CCAuNPs in figures 3(c) and (f), respectively. Such multipolar plasmons [10] also induced broadened and red-shifted resonance spectrum.

4. Transient absorption spectroscopic characterization

Femtosecond pump-probe measurements were performed on the AuFilm, the AuNPs, and the CCAuNPs. The pump pulses at 800 nm have a duration of about 150 fs, a repetition rate of 1 kHz, a maximum pulse energy of 1 mJ, and a beam diameter of about 5 mm on the sample surface. The probe pulses were produced by sending a portion of the 800 nm pulses to a quartz cell containing heavy water with a thickness of 1 mm, which have a beam diameter of about 400 μm on the sample surface and a bandwidth ranging from 300 to 1200 nm. Transient absorption (TA) spectrum (ΔA) was measured as a function of time delay ($\Delta\tau$) between the pump and probe pulses. A pump fluence of 360 μJ cm⁻² has been used in the transient absorption measurements in this work. To ensure the validness of this, we measured the absorption coefficient for the AuNPs and the CCAuNPs using femtosecond pulses with different power densities at 800 nm, which should have included some of the scattering process and is defined as

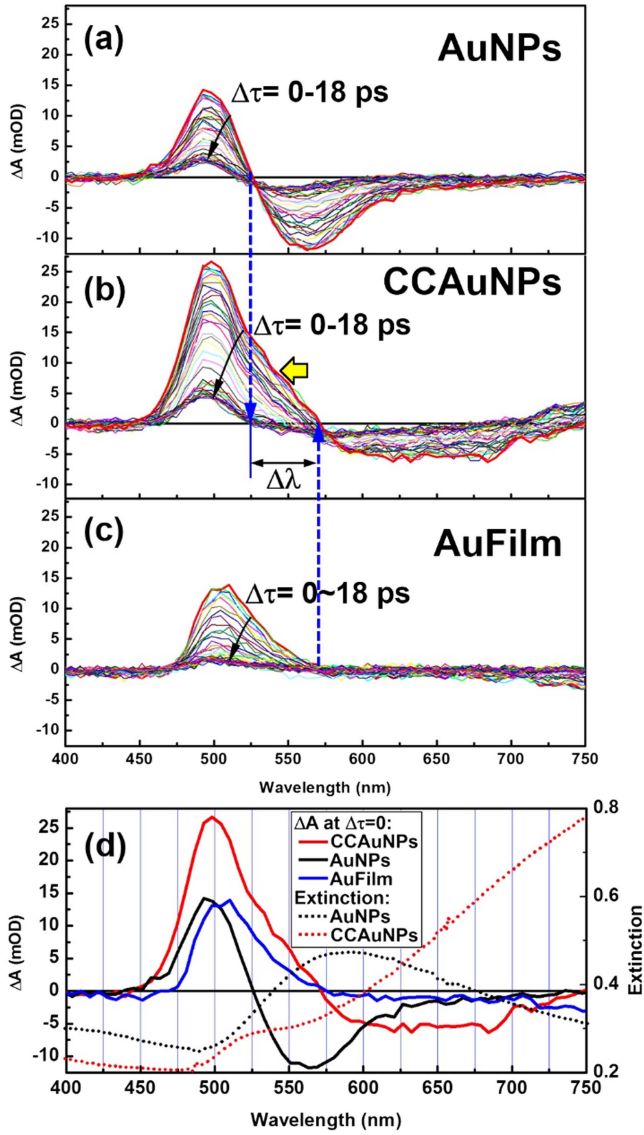


Figure 4. Transient absorption spectra at different time delays (0–18 ps) for (a) AuNPs, (b) CCAuNPs, and (c) AuFilm. (d) The transient absorption spectra at $\Delta\tau = 0$ measured on AuNPs (black), CCAuNPs (red), and AuFilm (blue) with the steady-state optical extinction spectra for AuNPs (dotted black) and CCAuNPs (dotted red) included for comparison.

$\eta = (I_{in} - I_R - I_T) / I_{in}$ with I_{in} , I_R , and I_T denoting the input, the reflected, and the transmitted light intensity, respectively. The value of η was measured to be roughly constant at 34% and 26% for the AuNPs and the CCAuNPs, respectively, when the pump fluence was increased from about 200 to 2000 $\mu\text{J cm}^{-2}$. These values not only verify a small difference between the optical absorbance by these two samples, but also indicate excellent linearity in a large range of pump fluences, which covers the used pump fluence of 360 $\mu\text{J cm}^{-2}$ and thus ensures validness of using such a similar pump fluence in the TA measurements.

Figures 4(a)–(c) show the transient absorption spectra $\Delta A(\lambda)$ at different time delays from 0 to 18 ps measured on AuNPs, CCAuNPs, and AuFilm, respectively. Figure 4(d) shows the transient spectra at a zero time delay ($\Delta\tau = 0$) for

samples of AuNPs (black), CCAuNPs (red), and AuFilm (blue). For comparison, the optical extinction spectra measured on the AuNPs and CCAuNPs are included in figure 4(d) by the dotted black and red curves, respectively. Comparing the solid with the dotted curves in black and red, we can conclude that the transient absorption spectra at $\Delta\tau = 0$ mainly resulted from the ‘bleaching’ of the optical extinction by the AuNPs under strong excitation by the pump pulses. As shown in figure 4, positive TA can be observed in spectral range of shorter wavelengths, which extends from about 450 to 525 nm in figure 4(a), from about 450 to 570 nm in figure 4(b), and from about 475 to 570 nm in figure 4(c). These features actually correspond to the rapid decrease in optical reflection and optical extinction due to the strong interband transitions for photon energies above the threshold. Clearly, this threshold energy is slightly different for different kinds of gold nanostructures and films, as can also be observed in figures 2 and 4(d), where the threshold energies/wavelengths are 2.54 eV/487 nm, 2.43 eV/509 nm, and 2.49 eV/498 nm for the AuNPs, the AuFilm, and the CCAuNPs, respectively. ‘Bleaching’ of this transition features as rapid ‘decrease’ in optical extinction exhibits as an ‘increase’ in transient absorption. However, the transient bleaching of LSPR, which exhibits as enhanced optical extinction, is observed as negative TA spectra, as shown in figure 4(a) from 525 to longer than 625 nm and in figure 4(b) from 570 to longer than 700 nm. Such performance cannot be observed with the continuous gold film, as can be verified by figure 4(c). Furthermore, the ‘bleaching’ process is generally accompanied by the red-shift and broadening of the LSPR spectrum [18], which may be attributed to electron–electron and electron–phonon interaction processes [19]. The TA spectra in figures 4(a) and (b) already combined multiple processes involving bleaching, red-shifting, and broadening of the spectroscopic resonance of the gold nanostructures.

Obviously, the spectroscopic response in figure 4(b) is not a simple superimposition of those in figures 4(a) and (c). The plasmonic coupling between the AuNPs and the continuous gold film induced by the conductive connection has not only enhanced the intensity, but also expanded significantly the bandwidth of the TA spectra, as inferred by a comparison between figures 4(a)–(c). The TA spectra for AuNPs extends from 450 to 525 nm with positive amplitudes and from 525 to longer than 625 nm with negative TA values, as shown in figure 4(a). This also implies that all of the TA spectra cross over a common intersection point on the axis of $\Delta A = 0$ at about $\lambda_1 = 525$ nm. However, the measurements on the AuFilm show a intersection of the falling edges of all of the TA spectra with the axis of $\Delta A = 0$ at about $\lambda_2 = 570$ nm, as shown in figure 4(c). Negligibly small TA signals with negative values can be observed at wavelengths shorter than 450 nm and longer than 570 nm for the TA measurements on the AuFilm. Thus, all of the TA spectra can be considered to have positive amplitudes and extend in the spectral range from 450 to 570 nm. Therefore, the TA spectra in figure 4(c) show only the bleaching effects of the optical extinction by the AuFilm and nearly no red-shift effects of the LSPR spectrum can be observed with the continuous AuFilm.

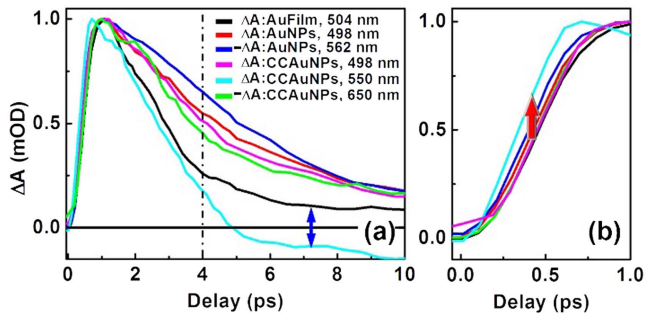


Figure 5. (a) Comparison between transient absorption dynamics between 40 nm-thick continuous gold film (AuFilm), isolated nanoparticles (AuNPs), and conductively connected gold nanoparticles (CCAuNPs) at typical wavelengths. (b) Local enlargement of the TA dynamics in (a) to show the faster rising time for the CCAuNPs at 550 nm.

These observations help resolve how the continuous AuFilm coating influences the LSPR of the AuNPs.

Interestingly, the TA spectra measured on the CCAuNPs show two intersection points of the falling edges with the axis of $\Delta A = 0$, which are located at $\lambda_1 = 525$ nm and $\lambda_2 = 570$ nm, introducing a transition band from positive to negative values of ΔA , as shown in figure 4(b) and indicated by the two dashed arrows. Thus, this transition band in the TA spectra is defined by the interaction between the AuNPs and the AuFilm.

It should be noted that the intersection points at $\lambda_1 = 525$ nm and $\lambda_2 = 570$ nm were observed at different delays of $\Delta\tau > 18$ ps and $\Delta\tau = 0$, respectively. This is because the TA signal decays much faster for the AuFilm than for the AuNPs, as can be observed in figures 4(a) and (c). At $\Delta\tau = 0$, these two intersection points are not overlapped, however, the one at $\lambda_2 = 570$ nm is exactly located at the transition point from positive to negative values of ΔA , as shown by the red curve in figure 4(b). With the increasing of $\Delta\tau$, the intersection point shifted to the left (shorter wavelengths), or the negative TA band expanded to cover the shorter-wavelength spectrum, as indicated by the yellow arrow to the left. Due to the slower response of the AuNPs than the AuFilm, the ‘remaining’ TA spectrum was dominated by the response of the AuNPs, because the TA response of the AuFilm reduced to nearly zero at $\Delta\tau > 18$ ps, as can be observed by comparing figures 4(a)–(c). The above mechanisms led to a much shortened relaxation time in the spectral range defined by λ_1 and λ_2 with $\Delta\lambda = \lambda_2 - \lambda_1$, as shown in figure 5.

Figure 5(a) shows the normalized TA dynamics at typical wavelengths measured on the samples of AuFilm, AuNPs, and CCAuNPs. For the AuFilm, the peak wavelength of the TA spectra at about 504 nm has been chosen as the typical wavelength, as shown by the black curve. For the AuNPs, the peak and valley-bottom wavelengths at 498 and 562 nm were chosen as the typical wavelengths, as shown by the red and blue curves. For the convenience of comparison, the TA dynamics at 562 nm has been inverted using $-\Delta A$. For the CCAuNPs, three typical wavelengths at 498, 550, and 650 nm

have been chosen to plot the TA dynamics, which are the peak wavelengths of the positive range (magenta), the center wavelength of the positive-to-negative transition region (light blue), and the center wavelength of the valley region (green) of the TA spectra, respectively. Again, the dynamics curve has been inverted by $-\Delta A$ at 650 nm for the convenience of comparison.

As shown in figure 5(a), all of the dynamic curves have different relaxation times with $\tau_{550\text{nm}} < \tau_{504\text{nm}} < \tau_{650\text{nm}} < \tau_{498\text{nm}} < \tau_{562\text{nm}}$. Fitting the dynamics data in figure 5(a) in the delay-time range of 0–4 ps, we obtained $\tau_{550\text{nm}} = 1.9$ ps, $\tau_{504\text{nm}} = 2.1$ ps, $\tau_{650\text{nm}} = 3.4$ ps, $\tau_{498\text{nm}} \approx 4.5$ ps, and $\tau_{562\text{nm}} = 5.1$ ps. The relaxation time scale at 498 nm is nearly the same for the AuNPs and CCAuNPs. Clearly, the isolated AuNPs has the longest relaxation dynamics among the three types of samples. The dynamics measured on the CCAuNPs has the shortest relaxation time in the transitional spectral region between λ_1 and λ_2 , implying strong modulation on LSPR of the AuNPs by the continuous gold film. The corresponding dynamics was reduced by a factor of up to 2.7 in its relaxation time due to conductive connection by the gold film.

The mechanisms can be understood by considering that the conductive connection led to the broadening and red-shift of LSPR of the AuNPs. Optical excitation by femtosecond pulses induced bleaching and transient red-shift of the coupled LSPR of the CCAuNPs, leaving a negative TA signal in the spectral band from 570 to longer than 750 nm at $\Delta\tau = 0$. This negative band receded quickly to shorter wavelength with time delay, resulting in a high-contrast and much faster TA dynamics within the transition spectral band between the positive and negative TA spectrum.

Furthermore, a shorter rising time can also be observed with the dynamics at 550 nm by the light blue curve in figure 5(b), as indicated by the upward arrow. This effect combines with the process that the falling edge reduces across the axis of $\Delta A = 0$ to become negative as the delay time increases, as shown in figure 5(a). These features enhanced the contrast and the absolute amplitude of the dynamics curve, which favored the speed-up of the optical switching effect.

5. Conclusions

In summary, we investigated the ultrafast optical modulation on LSPR of AuNPs by the conductive connection using a continuous gold film. The intensity, the bandwidth, and the speed of the relaxation dynamics of the LSPs in the structures were modulated differently in different spectral bands. Optical extinction bleaching and red-shift of LSPR have been the main responsible mechanisms. Electron–electron and electron–phonon scattering processes have been the main physical processes in the interaction between the laser pulses and the plasmonic nanostructures and in the excitation of LSPR. A much speed-up of the optical switching effect may be

achieved with steeper rising and falling edges or much enhanced contrast through conductive connection of the isolated AuNPs. This is based on the ultrafast redistribution of the free electrons between the AuNPs and the surrounding AuFilm, where the electronic dynamics is much faster in the AuFilm than in the AuNPs. Thus, the faster electronic decay in the continuous film reduced the response dynamics of localized oscillation of the plasmonic electrons in the AuNPs through close interactions. Such an effect was found to take place within a transition band defined by the delayed transient spectroscopic response of the AuFilm and the isolated AuNPs. The revealed mechanisms supplied applicable approaches to tailor the behaviors or optimize the designs of plasmonic optical switching devices.

Acknowledgments

We acknowledge the National Basic Research Program of China (2013CB922404), the National Natural Science Foundation of China (11574015, 11434016), and the Beijing Key Lab of Microstructure and Property of Advanced Materials for the support.

ORCID iDs

Xinping Zhang  <https://orcid.org/0000-0001-6534-0004>

References

- [1] Orendorff C J, Sau T K and Murphy C J 2006 Shape-dependent plasmon-resonant gold nanoparticles *Small* **2** 636–9
- [2] Hermoso W, Alves T V, Oliveira C C S D, Moriya E G, Ornellas F R and Camargo P H C 2013 Triangular metal nanoprisms of Ag, Au, and Cu: modeling the influence of size, composition, and excitation wavelength on the optical properties *Chem. Phys.* **423** 142–50
- [3] Mock J J, Barbic M, Smith D R, Schultz D A and Schultz S 2002 Shape effects in plasmon resonance of individual colloidal silver nanoparticles *J. Chem. Phys.* **116** 6755–9
- [4] Willets K A and Duyne R P V 2007 Localized surface plasmon resonance spectroscopy and sensing *Annu. Rev. Phys. Chem.* **58** 267–97
- [5] Liao H, Nehl C L and Hafner J H 2006 Optical properties of star-shaped gold nanoparticles *Nano Lett.* **6** 683–8
- [6] Mongin D, Baida H and Christofilos D 2011 Ultrafast nonlinear optical response of a single gold nanorod near its surface plasmon resonance *Phys. Rev. Lett.* **107** 057402
- [7] Inouye H and Tanaka K 1998 Ultrafast dynamics of nonequilibrium electrons in a gold nanoparticle system *Phys. Rev. B* **57** 11334
- [8] Zhu J, Li J and Zhao J 2011 Tuning the dipolar plasmon hybridization of multishell metal-dielectric nanostructure: gold nanosphere in a gold nanoshell *Plasmonics* **6** 527–34
- [9] Liu F, Zhang X, Fang X and Lin Y 2016 Plasmonic microcavity using photo-reduced silver nanoparticles and light-emitting polymer *Opt. Express* **24** 1747–57
- [10] Lin Y and Zhang X 2017 Ultrafast multipolar plasmon for unidirectional optical switching in a hemisphere-nanoshell array *Adv. Opt. Mater.* **5** 1601088
- [11] Liu F, Zhang X and Fang X 2017 Plasmonic plano-semicylindrical nanocavities with high-efficiency local-field confinement *Sci. Rep.* **7** 4007
- [12] Farhang A, Bigler N and Martin O J 2013 Coupling of multiple LSP and SPP resonances: interactions between an elongated nanoparticle and a thin metallic film *Opt. Lett.* **38** 4758–61
- [13] L  v  que G and Martin O J F 2006 Optical interactions in a plasmonic particle coupled to a metallic film *Opt. Express* **14** 9971–81
- [14] Link S and El-Sayed M A 1999 Size and temperature dependence of the plasmon absorption of colloidal gold nanoparticles *J. Phys. Chem. B* **103** 4212–7
- [15] Zhang X, He J, Wang Y and Liu F 2016 Terahertz beat oscillation of plasmonic electrons interacting with femtosecond light pulses *Sci. Rep.* **6** 18902
- [16] Liu H, Zhang X and Gao Z 2010 Lithography-free fabrication of large-area plasmonic nanostructures using colloidal gold nanoparticles *Photonics Nanostruct.: Fundam. Appl.* **8** 131–9
- [17] Zhang X, Liu H and Feng S 2009 Solution-processible fabrication of large-area patterned and unpatterned gold nanostructures *Nanotechnology* **20** 425303
- [18] Zhang X, Wang H, Wang M, Lin Y and Song X 2016 Ultrafast particle-plasmon enhancement by energy-band modification in nanostructured tungsten carbide *Opt. Express* **24** 22730–40
- [19] Bigot J Y, Halt   V, Merle J C and Daunois A 2000 Electron dynamics in metallic nanoparticles *Chem. Phys.* **251** 181–203